SALT observations of the Chromospheric Activity of Transiting Planet Hosts: Mass Loss and Star Planet Interactions

MNRAS **000**, 1–12 (2016) Preprint 7 December 2016 Compiled using MNRAS LATEX style file v3.0

SALT observations of the Chromospheric Activity of Transiting Planet Hosts: Mass Loss and Star Planet Interactions⋆⋆

D. Staab[1]†, C.A. Haswell[1], Gareth D. Smith[1], L. Fossati[1,2], J.R. Barnes[1], R. Busuttil[1] and J.S. Jenkins[3]

[1] *Department of Physical Sciences, The Open University, Walton Hall, Milton Keynes, MK7 6AA, UK*
[2] *Space Research Institute, Austrian Academy of Sciences, Schmiedlstrasse 6, Graz, A-8042, Austria*
[3] *Departamento de Astronomía, Universidad de Chile, Casilla 36-D, Las Condes, Santiago, Chile*

Accepted 2016 December 2. Received 2016 December 1; in original form 2016 January 29

ABSTRACT

We measured the chromospheric activity of the four hot Jupiter hosts WASP-43, WASP-51/HAT-P-30, WASP-72 & WASP-103 to search for anomalous values caused by the close-in companions. The Mount Wilson Ca II H & K S-index was calculated for each star using observations taken with the Robert Stobie Spectrograph at the Southern African Large Telescope. The activity level of WASP-43 is anomalously high relative to its age and falls among the highest values of all known main sequence stars. We found marginal evidence that the activity of WASP-103 is also higher than expected from the system age. We suggest that for WASP-43 and WASP-103 star-planet interactions (SPI) may enhance the Ca II H & K core emission. The activity levels of WASP-51/HAT-P-30 and WASP-72 are anomalously low, with the latter falling below the basal envelope for both main sequence and evolved stars. This can be attributed to circumstellar absorption due to planetary mass loss, though absorption in the ISM may contribute. A quarter of known short period planet hosts exhibit anomalously low activity levels, including systems with hot Jupiters and low mass companions. Since SPI can elevate and absorption can suppress the observed chromospheric activity of stars with close-in planets, their Ca II H & K activity levels are an unreliable age indicator. Systems where the activity is depressed by absorption from planetary mass loss are key targets for examining planet compositions through transmission spectroscopy.

Key words: circumstellar matter – stars: activity. individual: WASP-43, WASP-51, WASP-72, WASP-103.

1 INTRODUCTION

Stars with convective envelopes exhibit a wide range of magnetic activity levels, and consequently vary substantially in their chromospheric emission. The Mount Wilson program (Wilson 1968, Duncan et al. 1991) established the emission strength of the Ca II H & K line cores as the most widespread metric of chromospheric activity, using the S-index, a ratio between Ca II H & K emission flux and continuum passbands. A conversion from S-values to $\log(R'_{\rm HK})$ (Noyes et al. 1984) allows consistent comparison of stars with differing spectral types and has been measured for thousands of bright stars (e.g. Jenkins et al. 2011; Isaacson & Fischer 2010; Lovis et al. 2011). To first order, the stellar activity level depends on the stellar rotation rate and therefore age, with a particularly rapid decrease during spin-down over the first $\sim$ 1 Gyr (e.g. Mamajek & Hillenbrand 2008, hereafter MH08, and Pace 2013); $\log(R'_{\rm HK})$ is thus used as a stellar age indicator.

Knutson et al. (2010) published $\log(R'_{\rm HK})$ measurements for a sample of hot Jupiter (HJ) host stars, and concluded that there was a correlation between stellar activity and the presence of a temperature inversion in the planetary atmospheres. The latter was quantified with a model-independent metric based on the slope of the HJ secondary eclipse spectra. Hartman (2010) used the same sample to highlight a correlation between planetary surface gravity and

⋆ Based on observations made with the Southern African Large Telescope (SALT), under programs 2013-2-UKSC-010, 2014-1-UKSC-OTH-001, 2014-2-SCI-049 (PI: C.A.Haswell)

† E-mail:daniel.staab@open.ac.uk

$\log(R'_{\rm HK})$. The effect of the activity driven stellar high energy (XUV) flux on planetary atmospheres has been considered by e.g. Lammer et al. (2003); Erkaev et al. (2007); Lopez et al. (2012); Koskinen et al. (2013); Jin et al. (2014); Chadney et al. (2015). There has been significant interest in the chromospheric Ca II H & K line flux in HJ host stars, with the hypotheses that:

(i) A HJ planet can stimulate stellar activity through magnetic and/or tidal star planet interactions (SPI; Cuntz et al. 2000).

(ii) A HJ planet can suppress stellar activity through tidal interactions (Miller et al. 2012; Pillitteri et al. 2014).

(iii) Mass loss from a HJ planet can form a diffuse circumstellar gas cloud which absorbs in the cores of strong resonance lines (e.g. Ca II H & K and Mg II h & k) suppressing the measured stellar activity below its true value (Haswell et al. 2012; Fossati et al. 2013).

It is important to identify individual systems where mass loss appears to be masking the intrinsic activity, and cases where the stellar activity appears boosted by SPI. Ca II H & K emission enhancements from SPI should be a good predictor of a system's radio brightness (e.g. See et al. 2015). With dramatic enhancements in radio astronomy capabilities (ALMA, Partnership et al. 2015; LOFAR, van Haarlem et al. 2013; HERA, Hewitt 2011; SKA, Carilli & Rawlings 2004), detections of exoplanetary radio emissions are imminent (Vidotto et al. 2015). Radio observations are expected to yield planet rotation periods and magnetic moments, with important implications for exoplanetary magnetospheric physics and the transfer of energy and angular momentum between the host star and planet.

Systems where the Ca II H & K emission is absorbed by gas lost from the planet offer the potential to determine the planet's chemical composition through transmission spectroscopy. In WASP-12, while the diffuse gas is present at all observed phases, it produces the most near-UV absorption close to transit (Haswell et al. 2012). Differencing the observed spectrum near transit and away from transit can reveal the additional absorption from the densest regions of the gas shroud. Because the near-UV is such an informative wavelength region, with strong resonance lines of many abundant elements and ions, it is vital to make Hubble Space Telescope observations of the shrouded systems. There is no alternative means to obtain comparable information on planetary composition.

There are few southern hemisphere spectrographs calibrated to produce $\log(R'_{\rm HK})$, and large telescopes or significant exposure times are required to achieve sufficient signal to noise in the Ca II H & K cores of typical HJ host stars (V= 11 or fainter). We report observations using the Robert Stobie Spectrograph (RSS) at the Southern African Large Telescope (SALT), calibrating it to measure $\log(R'_{\rm HK})$, and results for four HJ host stars. Section 2 describes observations and data reduction; Section 3 describes the calibration; Section 4 discusses our planet host measurements in the context of large stellar samples and the three hypotheses listed above; Section 5 gives our conclusions and implications for future work.

2 OBSERVATIONS AND REDUCTION

Our observations were taken with the Robert Stobie Spectrograph (RSS; Kobulnicky et al. 2003), a multimode instrument at the Southern African Large Telescope (SALT; Buckley et al. 2006). Jenkins et al. (2011) assessed the effect of spectral resolution on the precision of $\log(R'_{\rm HK})$ measurements, finding a resolving power of R > 2500 is needed. We selected RSS settings to achieve the highest possible resolution in the region of the Ca II H & K lines: a 0.6″slit, and the PG3000 grating, with a camera station angle of 79.75° and grating angle of 39.875°. This yielded coverage from 3882 Å to 4614 Å, and a resolution R ∼ 7300 at 4000 Å. Prebinning of 2 in the spectral direction gave 0.23 Å per binned pixel. Future $\log(R'_{\rm HK})$ measurements with the RSS using our calibration should adopt the same setup to ensure consistency.

To permit calibration on the Mount Wilson system, we selected calibration stars from Baliunas et al. (1995), hereafter B95. B95 reported both the variability and the mean of S-values, $< S_{\rm MW} >$, using decades of data from the Mount Wilson survey. We included stars ranging from very inactive, $< S_{\rm MW} > = 0.14$, to very active, $< S_{\rm MW} > = 0.5$, (Table 2), chosen for low variability and $0.4 < B - V < 1.0$. HD 10700 and HD 22049 showed stable activity for a decade after B95's observations (Hall et al. 2007). We took 4 - 6 consecutive, short (15s - 70s), high SNR exposures, to avoid saturation of our calibration star spectra.

Our four science targets, WASP-43, WASP-51/HAT-P-30, WASP-72, and WASP-103 (Hellier et al. 2011; Johnson et al. 2011; Gillon et al. 2013; Gillon et al. 2014; Table 1), are host stars of transiting HJ planets. They were all discovered after 2010 and are notable for proximity to their host stars. WASP-103 b almost fills its Roche lobe (Figure 1); we made multiple exposures of this target to search for possible variations in circumstellar absorption of Ca II H & K.

Tables 2 and 3 summarise the observations. The calibrators HD 26913 and HD 26923 are separated by ∼ 40 arcsec, and were therefore observed simultaneously by appropriately orientating the RSS slit. The SALT pipeline (Crawford et al. 2010) performs corrections for CCD bias, gain and crosstalk between the CCD amplifiers. We performed flat fielding, background subtraction and wavelength calibration in IRAF, using arc-lamp exposures taken immediately after each target. Spectra were optimally extracted with particular attention to background subtraction and shifted into the stellar rest frame by cross-correlation with the National Solar Observatory solar spectrum (Kurucz et al. 1984), degraded to the RSS spectral resolution. All spectra have SNR > 15 in the Ca II H & K line cores. We rebinned all spectra to a common wavelength scale with 0.05 Å bin width, while conserving flux.

3 ANALYSIS

3.1 Extraction of instrumental S-values

We performed synthetic photometry using the Ca II H & K core bandpasses, H and K, and continuum windows, R and V, shown in Fig. 2. V and R are the mean flux values in 20 Å wide continuum windows centered on 3901.07 Å and 4001.07 Å while H and K are the core bandpasses, centered

Table 1. Stellar and planetary parameters relevant for this work, taken from TEPCAT (Southworth 2011), including stellar effective temperature ($T_{\rm eff}$), semi-major axis (a), orbital period and planetary equilibrium temperature ($T_{\rm eq}$).

System	$T_{\rm eff}$ (K)	a (AU)	Period (d)	$M_{\rm p}$ ($M_{\rm J}$)	$R_{\rm p}$ ($R_{\rm J}$)	$g_{\rm p}$ (ms^{-2})	$T_{\rm eq}$ (K)
HAT-P-30/WASP-51	6338 ± 42	0.042	2.81	0.71 ± 0.03	1.34 ± 0.07	9.8 ± 0.9	1630 ± 42
WASP-43	4520 ± 120	0.015	0.81	2.03 ± 0.05	1.04 ± 0.02	47.0 ± 1.4	1440 ± 40
WASP-72	6250 ± 100	0.037	2.23	1.46 ± 0.06	1.27 ± 0.20	22.9 ± 7.3	2210 ± 120
WASP-103	6110 ± 160	0.020	0.93	1.47 ± 0.11	1.55 ± 0.05	15.1 ± 0.9	2495 ± 66

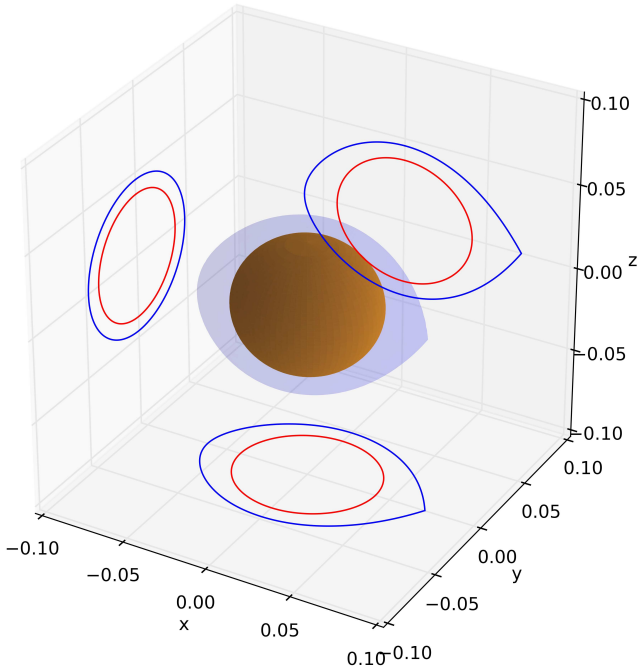

Figure 1. The Roche lobe (blue) of WASP-103b (orange), calculated using stellar and planetary parameters from TEPCAT (Southworth 2011). We corrected the empirical radius for the projection effect of a non-spherical planet viewed at orientation $i \neq 90°$, to give a self-consistent 3-D Roche geometry. Axes are in units of orbital separation, with the x and y axis in the orbital plane and z perpendicular to it. For the projections, red outlines represent the planet and blue outlines the Roche lobe.

on 3933.664 Å and 3968.47 Å, triangularly weighted with a FWHM of 1.09 Å. We followed Lovis et al. (2011) in using the (weighted) mean bandpass fluxes. This reduces edge effects from finite pixel size at the band boundaries, and makes a historical scaling factor obsolete. The instrumental S-index, $S_{\rm RSS}$, is given by

$$S_{\rm RSS} = \frac{H + K}{R + V}\ , \qquad (1)$$

Note flux-calibration is unnecessary for S-index measurements: the bandpass window placement makes these insensitive to the local spectral slope (e.g. Gray et al. 2003).

3.2 Calibration to Mount Wilson system

Table 2 reports the calibration measurements with propagated photon noise uncertainties on $S_{\rm RSS}$. For the B95 values, formal measurement uncertainty on $< S_{\rm MW} >$ is negligible compared to astrophysical stellar activity variation. The current activity level of our calibrators is uncertain so we report the variability range measured over the multi-decade baseline of B95 in Table 2 and Figure 3. The activity variability observed by B95 increases with the mean stellar activity level.

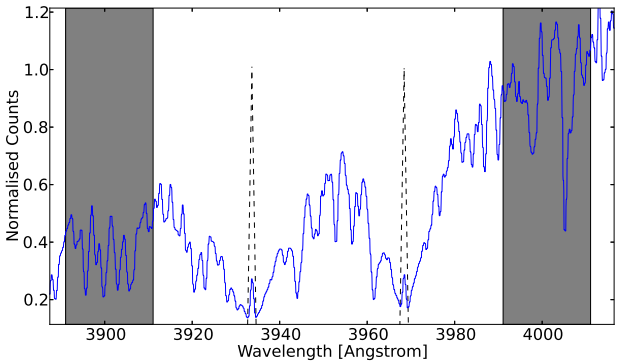

Figure 2. An RSS spectrum of our most active calibrator star, HD 22049, with continuum windows (greyed) and triangular core bandpasses highlighted. Strong Ca II H & K emission cores are evident. Counts are normalised to the mean of the red continuum bandpass.

Following Jenkins et al. (2011), we perform a simple linear calibration to the Mount Wilson system, using ordinary least squares fitting (Figure 3) obtaining:

$$S_{\rm RSS} = (0.60 \pm 0.02)\ S_{\rm MW} + (0.075 \pm 0.005). \qquad (2)$$

The RMS of the fit, 0.013, is at the level found in calibrations of other instruments (see Jenkins et al. 2006; Jenkins et al. 2008; Arriagada 2011). Scatter at the $\sim$ 5 % level is an unavoidable consequence of the long-term activity variation of calibration stars. Note that the high activity calibrators carry larger uncertainties and consequently less weight in the fit.

Table 3 lists $S_{\rm MW}$ for the planet hosts, calculated from Equations 1 and 2, and Figure 4 shows the Ca II H & K lines of our planet hosts. For the final conversion to $\log(R'_{\rm HK})$ following Noyes et al. (1984), the stellar B-V is required. No B-V measurements for WASP-103 have been published; Simbad[1] and the Exoplanet Orbit Database[2] (Han et al. 2014) report B-V colors for WASP-72 and WASP-51 that

[1] http://simbad.u-strasbg.fr/simbad/
[2] http://exoplanets.org/

Table 2. Calibrator star measurements and associated photon noise uncertainties. Mean Mount Wilson S-values and their variability range were taken from B95. Note that HD 26913 and HD 26923 were observed simultaneously.

Name	$< S_{\rm MW} >$	$S_{\rm RSS}$	HJD-2450000
HD 10700	0.171 ± 0.011	0.1781 ± 0.0001	6658.339
		0.1791 ± 0.0001	6658.340
		0.1794 ± 0.0001	6658.341
		0.1796 ± 0.0001	6658.342
HD 182101	0.216 ± 0.020	0.2139 ± 0.0004	6792.586
		0.2145 ± 0.0004	6792.587
		0.2143 ± 0.0004	6792.587
		0.2162 ± 0.0004	6792.588
HD 9562	0.136 ± 0.018	0.1444 ± 0.0002	6652.321
		0.1464 ± 0.0002	6652.322
		0.1451 ± 0.0002	6652.323
		0.1434 ± 0.0002	6652.324
HD 22049	0.496 ± 0.090	0.3465 ± 0.0009	6984.514
		0.3464 ± 0.0010	6984.514
		0.3465 ± 0.0011	6984.515
		0.3448 ± 0.0009	6984.515
		0.3458 ± 0.0006	6984.515
		0.3466 ± 0.0007	6984.516
HD 26913	0.396 ± 0.065	0.3002 ± 0.0072	6985.407
		0.2975 ± 0.0050	6985.407
		0.3174 ± 0.0023	6985.408
		0.3154 ± 0.0017	6985.409
HD 26923	0.287 ± 0.025	0.2390 ± 0.0015	6985.407
		0.2366 ± 0.0019	6985.407
		0.2381 ± 0.0010	6985.408
		0.2395 ± 0.0006	6985.409
HIP 110785	0.140 ± 0.015	0.1649 ± 0.0013	6803.656
		0.1649 ± 0.0011	6803.656
		0.1642 ± 0.0030	6803.657
		0.1607 ± 0.0037	6803.658
HIP 12114	0.226 ± 0.040	0.2050 ± 0.0005	6627.328
		0.2045 ± 0.0005	6627.328
		0.2029 ± 0.0005	6627.329
		0.2053 ± 0.0005	6627.330

are completely inconsistent with detailed spectral analyses in the discovery papers (Gillon et al. 2013 and Johnson et al. 2011). We calculated B-V for our planet hosts (Table 3) from the stellar parameters reported in TEPCAT, using Equation 3 in Sekiguchi & Fukugita (2000) propagating all uncertainties.

3.3 Uncertainty Budget

The $S_{\rm RSS}$ values measured for separate exposures of the same calibrator star agree to within 1%, with the single exception of 3% for HD 26913. With SNR $\sim$ 1500 at 4000 Å, there is a very small photon noise contribution to the calibration star $S_{\rm RSS}$ values. When we divide the RMS of the $S_{\rm RSS}$ values for each calibrator by the corresponding mean photon noise, a sharp rise above unity occurs below a photon noise level of $\sim$ 0.2 % due to a combination of astrophysical variability in the chromospheric emission and systematic uncertainties.

Our $S_{\rm MW}$ (Table 3) have uncertainties of 3 - 8%, largely dominated by the uncertainty from the calibration relation. Clearly the noise floor contribution of $\sim$ 0.2 % is negligible.

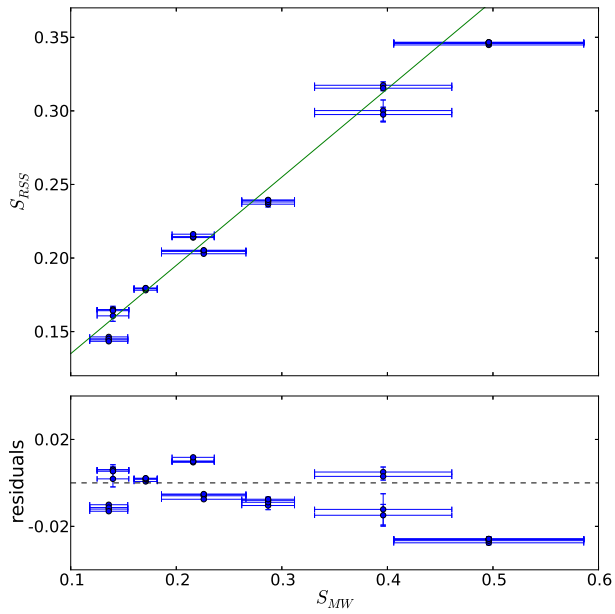

Figure 3. Calibration from instrumental to Mount Wilson S-values. Individual datapoints for each calibrator star overlap closely, and in most cases have $S_{\rm RSS}$ uncertainties smaller than the symbol sizes.

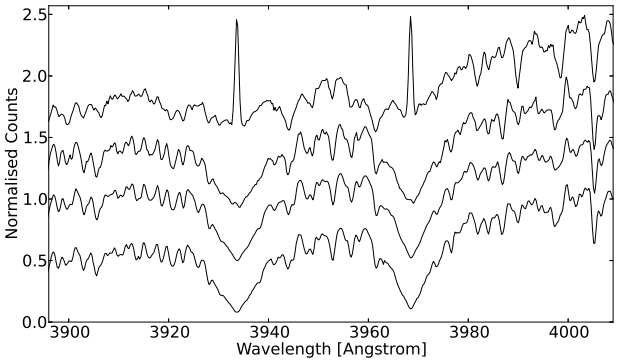

Figure 4. Spectra plotted in order of decreasing apparent activity from top to bottom: WASP-43, WASP-103, WASP-51, WASP-72. An arbitrary offset was added to the spectra for visibility. Counts are normalised to the mean of the red continuum bandpass.

The $\log(R'_{\rm HK})$ values listed in Table 3 incorporate the propagated errors on B-V, a significant contribution for WASP-43 which has a poorly constrained effective temperature. Obviously our $\log(R'_{\rm HK})$ values are snapshots during activity cycles and short-term variability. Gomes da Silva et al. (2014) used a sample of 271 mostly inactive stars, obtained over a $\sim$ 10 year timescale, to show that astrophysical variation in $\log(R'_{\rm HK})$ results in an RMS of typically 0.015 dex, and at most 0.08 dex. Our uncertainties render the typical astrophysical variability negligible.

Table 3. Planet host measurements and activity values derived from them. Note instrumental S-values report photon noise uncertainties, while $S_{\rm MW}$ includes the calibration uncertainty. B-V values and uncertainties are derived as described in Section 3. Orbital phases were calculated from ephemerides in TEPCAT, with phase 0 representing mid-transit. Stellar ages in the literature are compared with activity ages derived from the MH08 relation, using our $\log(R'_{\rm HK})$ values.

Name	HJD$_{-2450000}$	phase	$t_{\rm exp}$(s)	$S_{\rm RSS}$	$S_{\rm MW}$	B-V	$\log(R'_{\rm HK})$	activity age[a]	literature age[b]
WASP-43	6689.420	0.661	2032	1.209 ± 0.008	1.889 ± 0.065	1.10 ± 0.06	-4.17 ± 0.10	45 ± 40 Myr	300-600 Myr(1)
WASP-51	6698.410	0.883	1108	0.168 ± 0.001	0.155 ± 0.010	0.49 ± 0.01	-4.98 ± 0.07	6.2 ± 1.3 Gyr	0.5-1.8 Gyr(2)
									0.6-1.0 Gyr(3)
WASP-72	6606.307	0.332	1108	0.149 ± 0.001	0.124 ± 0.009	0.48 ± 0.03	-5.30 ± 0.15	11 ± 0.8 Gyr	2.6-3.8 Gyr(4)
WASP-103	6779.562	0.701	317	0.224 ± 0.003	0.248 ± 0.013	0.54 ± 0.05	-4.59 ± 0.04	950 ± 230 Myr[c]	1.8-6.2 Gyr(5)
	6779.566	0.706	317	0.221 ± 0.003	0.244 ± 0.013		-4.60 ± 0.04		3-5 Gyr(6)
	6779.573	0.713	317	0.221 ± 0.003	0.243 ± 0.013		-4.60 ± 0.04		
	6780.489	0.703	317	0.227 ± 0.003	0.253 ± 0.013		-4.57 ± 0.04		
	6780.493	0.707	317	0.227 ± 0.003	0.254 ± 0.013		-4.57 ± 0.04		
	6780.497	0.712	317	0.233 ± 0.003	0.263 ± 0.013		-4.55 ± 0.03		
	6780.501	0.716	317	0.230 ± 0.003	0.258 ± 0.013		-4.56 ± 0.04		
	6780.535	0.753	390	0.220 ± 0.009	0.241 ± 0.019		-4.61 ± 0.06		
	6790.473	0.490	390	0.228 ± 0.003	0.256 ± 0.013		-4.57 ± 0.04		
	6790.478	0.496	390	0.229 ± 0.003	0.257 ± 0.013		-4.56 ± 0.04		
	6790.482	0.500	390	0.235 ± 0.003	0.267 ± 0.013		-4.54 ± 0.03		
	6790.487	0.505	390	0.237 ± 0.003	0.269 ± 0.013		-4.53 ± 0.03		
	6790.502	0.521	390	0.227 ± 0.003	0.254 ± 0.013		-4.57 ± 0.04		
	6790.507	0.527	390	0.234 ± 0.003	0.264 ± 0.013		-4.54 ± 0.03		
	6790.511	0.531	390	0.225 ± 0.003	0.251 ± 0.013		-4.58 ± 0.04		
	6790.516	0.537	390	0.231 ± 0.003	0.260 ± 0.013		-4.55 ± 0.03		

[a] Uncertainty propagated from uncertainty in $\log(R'_{\rm HK})$. Note MH08 reports activity-age scatter at the 60% and 30 % levels for ages below and above 130 Myr respectively.
[b] (1)Hellier et al. 2011,(2)Johnson et al. 2011, (3)Bonfanti et al. 2015, (4)Gillon et al. 2013, (5)Southworth et al. 2014, (6)Gillon et al. 2014
[c] from mean of our measurements

4 DISCUSSION

Interest in $\log(R'_{\rm HK})$ for individual planet hosts is motivated by evidence it might provide regarding magnetic and tidal star-planet interactions and by the implications of the anomalously low values of $\log(R'_{\rm HK})$ of some HJ hosts stars.

4.1 Star-Planet Interactions

Stellar activity *enhancements* have been detected for individual HJ systems (e.g. Shkolnik et al. 2008; Pillitteri et al. 2011) and around periastron for a very eccentric system (Maggio et al. 2015). Null results for both chromospheric and coronal emission enhancements can be found in e.g. Poppenhaeger et al. (2010), Lenz et al. (2011) and Figueira et al. (2016). Activity *suppression* by a planet has been suggested by Miller et al. (2012) and Pillitteri et al. (2014) to explain the anomalously low X-ray and Ca II H & K line core emission of WASP-18. The parameters of this system, $M_P = 10.4\ M_{\rm J}$, $P = 0.9$ d, suggest a particularly strong tidal interaction. The magnitude of this effect should be greater than for any other HJ system, and may significantly affect the shallow stellar convective zone of the F6V host, depressing its magnetic dynamo (Pillitteri et al. 2014).

Several studies have investigated whether mean stellar activity levels are systematically influenced by the presence and properties of planetary companions across larger stellar populations. Results have been very mixed for both X-ray measurements (e.g. Scharf 2010 in comparison with Poppenhaeger & Schmitt 2011) and Ca II H & K data (e.g. Canto Martins et al. 2011 in comparison with Krejčová & Budaj 2012). It seems that at best optical and X-ray diagnostics reveal magnetic SPI effects in only a small subset of observations of short period planets. Tidal spin-up of host stars by orbital decay of HJs could play a more important, but nonetheless, limited role (Miller et al. 2015). The latter process would 'rejuvenate' the parent star, delaying or reversing the decline of rotation and activity with age. For a comprehensive overview of SPI studies and the most recent statistical work to date, see Miller et al. (2015). SPI detection in large samples of systems remains controversial and beset by selection biases. However, strong evidence for activity enhancements in individual cases has been found in particular for planet-hosting wide binary systems (Poppenhaeger & Wolk 2014). Theoretical work on magnetic SPI effects ranges from simple analytical approaches (e.g. Lanza 2008) to more sophisticated, three-dimensional MHD models (e.g. Strugarek et al. 2015). Studies such as Saur et al. (2013) and Lanza (2012) cannot account for the energy release observed for time-variable SPI signatures. Treatments which consider the dynamical behaviour of the magnetic field topology allow the phenomenon of magnetic reconnection to be included. Lanza (2012) finds that the power dissipated by reconnection between stellar and planetary fields at the planet's magnetospheric boundary is insufficient to explain observations attributed to SPI. In con-

trast, relaxation of stressed magnetic loops between stellar and planetary fields can provide sufficient power (Lanza 2013). Cohen et al. (2011) perform time-dependent MHD modelling, concluding that there is sufficient energy release from reconnection to explain observed SPI effects. These studies also provide explanations for the intermittent nature of magnetic SPI signatures seen in e.g. Shkolnik et al. (2008). However, both observational and theoretical work on SPI remain active areas of research without conclusive outcomes to date.

4.2 Circumstellar Absorption of Chromospheric Emission

Large-scale hydrodynamic escape of the upper atmosphere of irradiated short-period planets is predicted by models (Lammer et al. 2003; Bisikalo et al. 2013; Matsakos et al. 2015) and has been directly detected through transmission spectroscopy. Notable cases are the HJs HD 209458b (Vidal-Madjar et al. 2003) and HD 189733b (Lecavelier des Etangs et al. 2010; Bourrier et al. 2013) and the spectacular case of the warm Neptune GJ 436b (Kulow et al. 2014; Ehrenreich et al. 2015). Heavy species are entrained in these prodigious outflows of hydrogen (Linsky et al. 2010; Fossati et al. 2010; Haswell et al. 2012; Ben-Jaffel & Ballester 2013). Haswell et al. (2012) suggested that these outflows can feed diffuse circumstellar gas shrouds which absorb the stellar flux in the cores of strong lines of abundant species, depressing the chromospheric emission which arises in precisely these spectral lines. In particular this naturally explains the anomalous zero flux Mg II h & k line cores observed in the extreme HJ host WASP-12. Corroborating this, Fossati et al. (2013) showed that WASP-12's Ca II H & K lines have an extremely low value of $\log(R'_{\rm HK}) = -5.5$. If intrinsic to the star, this would be unique: WASP-12 is the lowest point shown in each panel of Figure 5. Occam's razor suggests this extreme observed property of the star WASP-12 must be related to the presence of its extreme HJ planet, WASP-12b.

This *apparent activity suppression* arises from planetary mass loss which is sensitive to the planet's surface gravity. There is a highly significant correlation between planetary surface gravity ($g_{\rm p}$) and stellar $\log(R'_{\rm HK})$ for close-in planets (Hartman 2010). Figueira et al. (2014) confirmed this, showing it is not due to selection biases. Lanza (2014) constructed a physical model reproducing the observed correlation, which was refined by Fossati et al. (2015a). Large-scale planetary mass loss akin to that inferred from apparent activity suppression may underly the sub-Jovian desert (Kurokawa & Nakamoto 2014; Lundkvist et al. 2016). Other explanations of this dearth in the known exoplanet population have been suggested however (Matsakos & Königl 2016 and references therein).

4.3 Activity values in context

Figure 5 shows our new $\log(R'_{\rm HK})$ measurements in the context of other transiting, short-period planet hosts (Figueira et al. 2014), and a large sample of field stars (Pace 2013). We limit all samples to 0.4 < B-V < 1.2 because $\log(R'_{\rm HK})$ is well calibrated in this range and notably unreliable for B-V > 1.2 (Noyes et al. 1984). Main sequence, subgiant and giant stars have very different activity distributions (e.g. Wright 2004; Mittag et al. 2013) so it is useful to place stars on the HR diagram and differentiate them by their evolutionary status. We used absolute magnitudes and reliable B-V values from the XHIP catalogue (Anderson & Francis 2012), combined with the Wright (2004) empirical average main sequence (MS), to calculate the height above the MS for each star. $\log(R'_{\rm HK})$ was calculated from the XHIP B-V data and the mean Pace (2013) S-values. We define an unevolved main sequence population of stars less than 0.45 mag above the MS, as in Wright (2004). A main sequence basal activity limit of $\log(R'_{\rm HK})$>-5.1 applies only to this sample, seen in Fig. 5a. Note this limit arises from chromospheric emission that is always present. It is the stellar analogue of the quiet sun chromospheric emission. The basal level is reached when stars are devoid of active regions (see e.g. Schröder et al. 2012 and references therein).

None of the planet hosts are highly evolved, so we reject objects more than 2.0 mag above the MS, and define a sample of moderately evolved stars between 0.45 and 2.0 mag above the MS, comprised mostly of subgiants (Fig. 5b). For most planet hosts, precise parallaxes are unavailable, so we cannot distinguish between MS and moderately evolved stars in the same way. We therefore compare planet hosts to both populations in Figure 5.

These comparisons indicate that transiting planet hosts have a greater spread in $\log(R'_{\rm HK})$ than field stars, a statement which remains true whether we consider main sequence or evolved stars. We performed Anderson-Darling tests, comparing the $\log(R'_{\rm HK})$ distribution of the planet host sample with our main sequence, evolved, and combined field star samples respectively. The resulting Anderson-Darling statistic values of 27.7, 8.2 and 8.6 correspond to very low probabilities (3×10^{-5}, 4×10^{-4}, 3×10^{-4}) that the samples are drawn from the same parent distribution in each case. We find that the Figueira et al. (2014) dataset contains 22 planet hosts below the basal chromospheric emission limit (24 % of the sample). Activity depression is widespread in the known population of transiting planet hosts. Only 2% of our unevolved sample and 9% of our combined field star sample, show such an unusual activity level. Fig. 6 identifies all planet hosts below the basal limit, more than doubling the number previously identified (Fossati et al. 2013). The horizontal basal envelope which is fairly clear in the main sequence field star sample in Fig. 5(a) becomes a diagonal envelope in Fig. 5(b), with higher $\log(R'_{\rm HK}) \sim -5.0$ for the bluest evolved stars and lower $\log(R'_{\rm HK}) \sim -5.2$ for the redder evolved stars (c.f. Mittag et al. 2013). WASP-72 and the outliers identified by Fossati et al. (2013) appear even more anomalous in the context of Fig. 5(b) than they do in the context of Fig. 5(a).

Anomalously low $\log(R'_{\rm HK})$ is seen for Kepler-25 and Kepler-68: two multi-planet systems each hosting 2 low-mass (0.02 -0.08 $M_{\rm J}$), short period companions. Tidal influences of these planets on their parent stars is negligible. Therefore, a tidal stellar activity suppression mechanism as proposed for WASP-18 by Miller et al. (2012) can certainly be excluded in these cases. Note that all anomalous planet hosts discussed fall below the chromospheric basal limit, but above $R_{\rm phot}$, the purely photospheric contribution to the Ca II H & K bandpasses. This is shown in Figure 7,

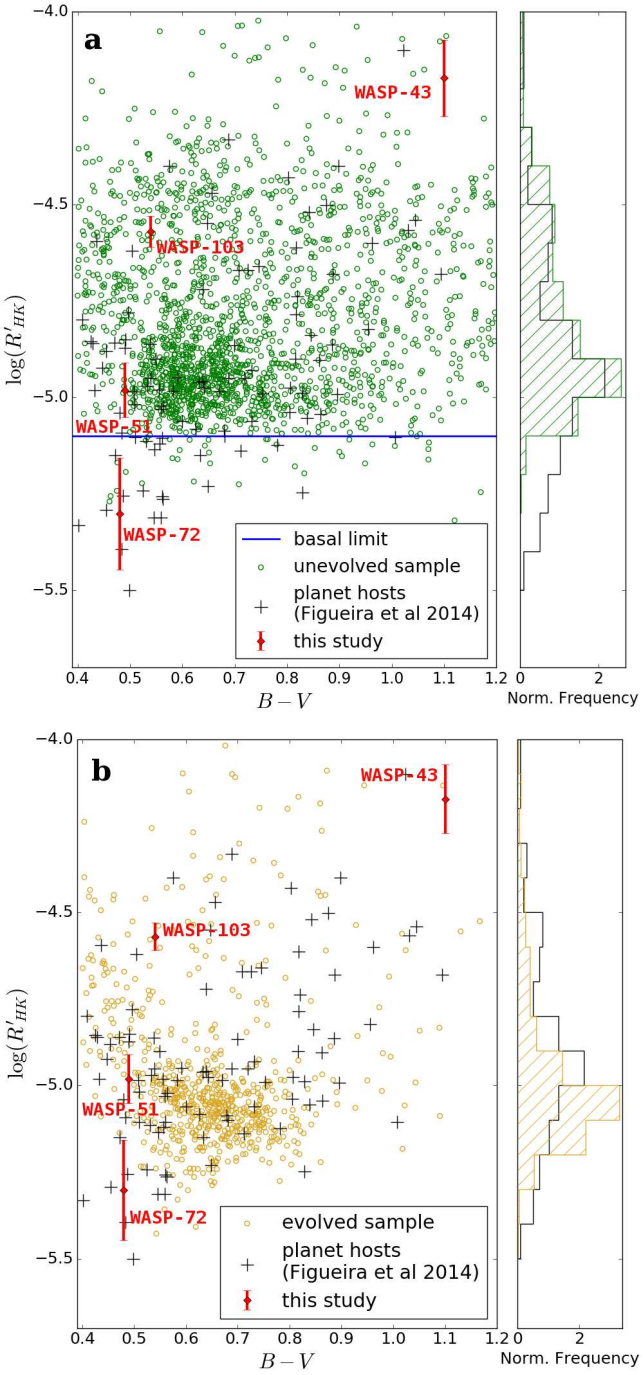

Figure 5. $\log(R'_{\rm HK})$ distribution for field stars compared to archival data on planet hosts and our measurements, using (a) unevolved, main sequence stars less than 0.45 mag above the average main sequence and (b) evolved field stars between 0.45 mag and 2 mag above the average main sequence. Note that bimodality in the distributions is expected (e.g Wright 2004, Gray et al. 2006).

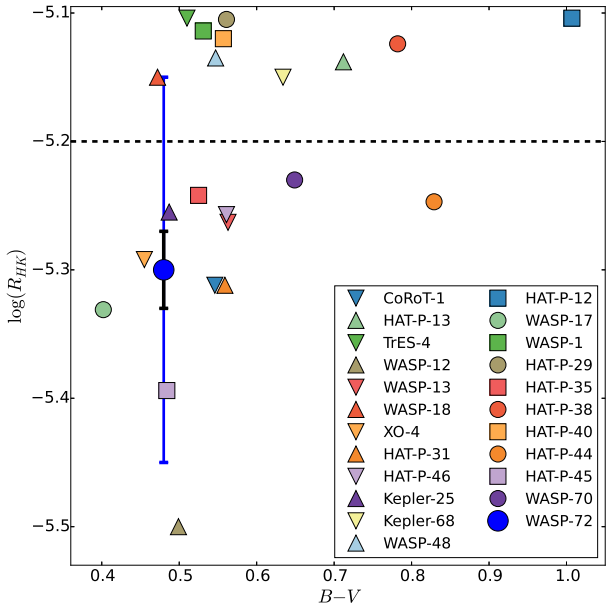

Figure 6. Short period planet hosts from Figueira et al. (2014) with $\log(R'_{\rm HK})$ below the main sequence basal limit (-5.1) and our measurement of WASP-72. For reference, we show the uncertainty with (blue) and without (black) the uncertainty in our calibration to the Mount Wilson system (Equation 2). Stars with $|\gamma - {\rm V_{ISM}}| < 15$ km s^{-1} (triangles) may be depressed below $\log(R'_{\rm HK}) = -5.2$ by ISM absorption.

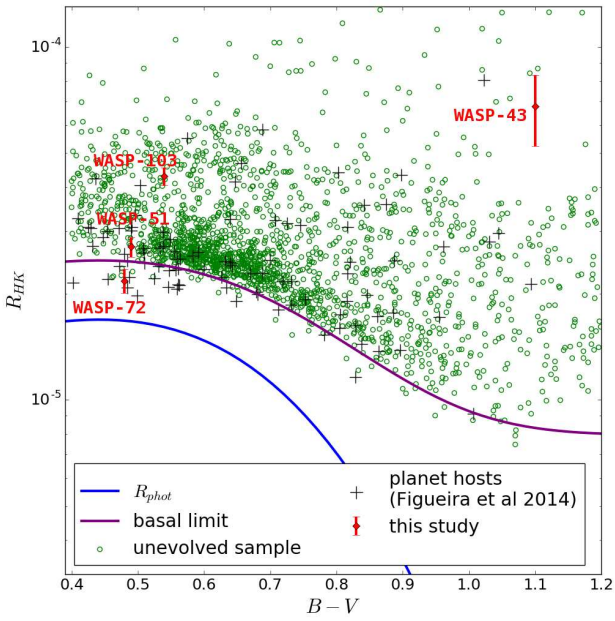

Figure 7. $R_{\rm HK}$ distribution for unevolved field stars and planet hosts, compared to the chromospheric basal limit and $R_{\rm phot}$, the photospheric contribution to $R_{\rm HK}$.

where we plot $R_{\rm phot}$ as defined by Noyes et al. (1984) and $R_{\rm HK} = R_{\rm phot} + R'_{\rm HK}$.

Transiting planet hosts are generally more distant than field stars with $\log(R'_{\rm HK})$ measurements. Thus an alternative explanation for $\log(R'_{\rm HK})$ depression in planet hosts is high absorption in the ISM along the line of sight. In

the case of WASP-12, this is unlikely (Fossati et al. 2013), but Fossati et al. (2015b) found that the ISM explanation is viable for WASP-13, while circumstellar absorption could also be present. To assess potential ISM absorption contributions for the planet hosts of interest, we calculated the difference between the systems' radial velocities, γ, and the velocities of known local ISM clouds, V_{ISM} (Table 4). We used the Redfield & Linsky (2008) ISM model[3], identifying ISM clouds traversed along the relevant lines of sight and calculating the clouds' projected radial velocities. ISM absorption can depress $\log(R'_{HK})$ values if the velocity differences are within the Ca II H & K core bandpass widths ($\pm$ 86 km/s). The effect is much more pronounced for smaller $|\gamma - V_{ISM}|$, amplified by the triangular H and K bandpass weighting (Fossati et al, in prep.). If we assume typical ISM column densities of log N_{CaII} = 12 (Welsh et al. 2010) for the relevant stellar distances (100-500 pc) and conservatively assume a star has intrinsic chromospheric emission exactly at the basal level, our calculations show that $|\gamma - V_{ISM}| \lesssim 15$ km s^{-1} is required to cause $\log(R'_{HK})$ values lower than -5.2 (Fossati et al, in prep.). We indicate $\log(R'_{HK}) = -5.2$ in Fig. 6, and differentiate objects with $|\gamma - V_{ISM}| \lesssim 15$ km s^{-1} from the remainder. Objects with $\log(R'_{HK}) < -5.2$ and $|\gamma - V_{ISM}| > 15$ km s^{-1} are those most likely to be exhibiting significant circumstellar absorption of the Ca II H & K line cores. Using the assumptions outlined above and the $|\gamma - V_{ISM}|$ values in Table 4, we expect values of the interstellar contribution to the $\log(R'_{HK})$ depression for individual stars to be $\sim$ 0.03 - 0.12 dex.

Table 4 and the line in Fig. 6 is only indicative of potential ISM contributions from known local clouds, mapped at low spatial resolution. A detailed case by case analysis (see Fossati et al. 2013 and Fossati et al. 2015b) is needed for all anomalous planet hosts to assess the ISM versus circumstellar absorption contributions. This needs to take into account the likely intrinsic activity levels in all cases, and is beyond the scope of the current work.

4.4 Findings for Individual Systems

4.4.1 WASP-43

WASP-43b orbits a K-type star with T_{eff} = 4520 K (Hellier et al. 2011) and is consequently less irradiated than most HJ planets with similar orbital proximity (c.f. Table 1). WASP-43 has a rotation period of 15.6 d, i.e. a gyrochronological age of 300-600 Myr (Hellier et al. 2011). This is consistent with its X-ray emission (Czesla et al. 2013), but tidal spin-up could affect both, obscuring the true system age. Our $\log(R'_{HK})$ value places WASP-43 at the activity level seen for very young (< 130 Myr; MH08) members of the Pleiades cluster and Sco-Cen association in Figure 5. WASP-43 lies well above the Hyades, $\sim$ 625 Myr, activity level at this spectral type; see Fig.4 in Paulson et al. (2002). The $\log(R'_{HK})$-age relation of MH08 gives a very low age (Table 3), inconsistent with WASP-43's gyrochronological age. The activity value is not significantly affected by erroneous extrapolation of our calibration to large S-values. To verify this, we compared our spectrum of WASP-43 with a HIRES spectrum of a similar star, HD 86856, with $\log(R'_{HK})$ = -4.37 and confirmed that WASP-43's core emission is higher by the amount expected from our $\log(R'_{HK})$ value.

MH08 found a tight correlation between stellar X-ray emission, parameterised by $\log(R_X)$, and $\log(R'_{HK})$. Using WASP-43's $\log(R_X) = -4.98 \pm 0.23$ (Czesla et al. 2013), equation A1 in MH08 predicts $\log(R'_{HK}) = -4.56 \pm 0.07$. Our measured value, $\log(R'_{HK}) = -4.17 \pm 0.10$ constitutes a clear outlier with respect to Figure 15 of MH08, far beyond the scatter among $\sim$ 200 stars therein. The X-ray activity level agrees with the stellar rotation period, and our $\log(R'_{HK})$ measurement is anomalously high. This could be due to a stellar flare during the exposure producing an increase in Ca II H & K emission by a factor of 2 to 3. Such short-term variability has been observed for the young, rapidly rotating K5V star BD+201790, which hosts a disputed HJ (Hernán-Obispo et al. 2010; Hernán-Obispo et al. 2015). However, stars similar to WASP-43 with 4000 K < T_{eff} < 5000 K; and 10d < P_{rot} < 20d have flare frequencies of 0.04 d^{-1} - 0.21 d^{-1} with durations of 0.1 - 15 hr (Balona 2015). This implies a < 14% chance of seeing a flare during our 0.56 hr exposure even at the most favourable flare frequencies and durations.

Our measurement was taken at WASP-43 b orbital phase 0.66, whereas the X-ray data from Czesla et al. (2013) covers the secondary eclipse of the planet. Shkolnik et al. (2008) observed clear Ca II H & K emission increases for the HJ host HD 179949 at phases 0.6 - 1 and attributed this to SPI. If WASP-43 shows similar behaviour, our data could be affected by SPI, whereas the X-ray data is not. The putative strong flaring event during our exposure could have been induced by SPI increasing the flaring frequency above that of stars without HJ companions. Only mixed evidence exists for Ca II H & K emission increases due to SPI at the few % level (Miller et al. 2015). The doubling or tripling implied by our measurement is unique, and requires confirmation.

Figure 8 shows all planets from the Exoplanet Orbit Database with $0.1 M_J < M_p$, $\sin i < 13 M_J$ and $a < 0.1$ AU, the hot Jupiters observed in this paper and several systems where evidence for SPI has been published. We plot the tidal SPI proxy h_{tide}/h_{scale}, following Cuntz et al. (2000), where h_{tide} is the height of the tidal bulge raised on the star, and h_{scale} is photospheric scale height (see also e.g. Poppenhaeger & Wolk 2014; Pillitteri et al. 2014). In the absence of detailed theoretical modelling and magnetic field maps, simple scaling proxies based on known system properties are the only available guide to assess putative magnetic SPI strength. Ideally, the maximum power released by magnetic reconnection would be calculated analytically following Lanza (2013). A meaningful estimate requires measurements of the stellar field strength and configuration, which are not available for our targets. It is worth noting that Miller et al. (2015) use $M_p \sin i/a^2$ as a magnetic SPI strength proxy, highlighting potential activity enhancement in "extreme" systems with $M_p \sin i/a^2 > 450$ (see their Fig. 7.) WASP-103 and WASP-43 have $M_p \sin i/a^2$ values 8 and 20 times larger than this threshold. However, this is not an ideal proxy to differentiate magnetic from tidal SPI effects: $M_p \sin i$ strongly correlates with h_{tide}/h_{scale} due to the $M_p \sin i$ dependence. It is also questionable to assume all close-in planets of interest orbit in the regime where the stellar field strength falls of as a^{-2}, since this will change with the geometry of

[3] http://lism.wesleyan.edu/LISMdynamics.html

Table 4. Differences between the stellar radial velocities (γ) and projected velocities of known ISM clouds (Redfield & Linsky 2008), traversed along the line-of-sight to each planet host below the chromospheric basal limit, and WASP-51. γ values were taken from the Exoplanet Orbit Database and the individual planet discovery papers.

System	γ (km s^{-1})	$\lvert\gamma - V_{ISM}\rvert$ (km s^{-1})	ISM clouds
CoRoT-1	23.8	3.2, 0.6	LIC, Aur
HAT-P-12	-40.6	34.7	NGP
HAT-P-13	14.8	0.3	LIC
HAT-P-29	-21.7	36.8	LIC
HAT-P-31	-2.4	14.7, 21.2, 26.5	LIC, Mic, Oph
HAT-P-35	41.0	24.2, 20.9	LIC, Aur
HAT-P-38	-19.7	37.4, 33.2	LIC, Hya
HAT-P-40	-25.0		none
HAT-P-44	-33.5	27.5	NGP
HAT-P-45	23.9	55.3, 50.6, 63.5	Oph, G, Aql
HAT-P-46	-20.9	10.0, 6.5, 21.5	Oph, G, Aql
Kepler-25	-8.5	2.9, 10.5, 5.0	LIC, Mic, G
Kepler-68	-20.9	13.2, 5.8	LIC, Mic
TrES-4	-15.9	1.8, 4.3	LIC, Mic
WASP-1	-13.4	22.6	LIC
WASP-12	18.9	3.2	LIC
WASP-13	9.9	2.7	LIC
WASP-17	-49.3	21.0	G
WASP-18	2.8	2.0, 27.3, 8.4	LIC, Dor, Cet
WASP-48	-19.7	14.2	LIC
WASP-70	-65.4	43.6	Mic
WASP-72	35.9	23.4, 17.8	LIC, G
XO-4	1.6	14.2	LIC
WASP-51	44.7	28.0, 24.8	LIC, Aur

the fields (see e.g. Lanza 2013). We choose to simply plot the semi-major axis in Figure 8 as an indicator of magnetic interaction strength. There is insufficient information about the stellar field environments for the vast majority of exoplanets to differentiate them into subsets of other parameterisations. Both proxies plotted are exceptionally favorable for the WASP-43 system. The alternative simple proxies used in the literature, such as $M_p \sin i/a^2$, $M_p \sin i/a$ and $M_p \sin i/P$ (Miller et al. 2015; Poppenhaeger et al. 2010; Shkolnik et al. 2008) also all indicate SPI is particularly likely for WASP-43. Note that WASP-43b and WASP-103 are the Hot Jupiters with the shortest and 4th shortest semi-major axis discovered to date.

Since our activity value is anomalously high with respect to the stellar rotation period, a tidal explanation (invoking enhanced rotationally-driven emission) is disfavored for WASP-43.

We find no evidence for circumstellar absorption in accordance with Salz et al. (2016)'s finding that WASP-43 b should be stable against mass loss. Time-variable magnetic SPI at an unprecedented level could be an explanation for our high value of $\log(R'_{HK})$. To distinguish this explanation from "normal", flare activity, phase-resolved monitoring of X-ray and/or optical activity indicators of WASP-43 is needed.

4.4.2 WASP-51/HAT-P-30

This planet is a typical spin-orbit misaligned HJ (Johnson et al. 2011; Enoch et al. 2011). The most precise literature ages (Table 3) are based on isochrone dating, using the stellar parameters of Johnson et al. (2011). The high stellar Li abundance is consistent with a $\leq$ 1 Gyr age (Enoch et al. 2011). Our $\log(R'_{HK})$ derived age (Table 3) is clearly anomalously high. In summary, it seems the true age is $\sim$ 1 Gyr and the normal stellar activity has been depressed, either through the planet tidally suppressing the stellar magnetic dynamo or through absorption of the Ca II H & K emission by circumstellar gas from the planet or by the ISM. The MH08 relation predicts $\log(R'_{HK}) \sim$ -4.6 at a 1 Gyr age.

If the intrinsic chromospheric emission is indeed at that level, our measurement implies depression of $\log(R'_{HK})$ by $\sim$ 0.4 dex. This is unlikely to arise from absorption in the ISM: our calculations show that clouds with $\lvert\gamma - V_{ISM}\rvert \lesssim$ 30 km s^{-1} and a column density log $N_{CaII} > 16$ would be required (Fossati et al, in prep). For stars out to 800 pc Welsh et al. (2010) consistently observe log $N_{CaII} < 13$ (typically $\sim$ 12), and WASP-51 lies at $\sim$190 pc (Johnson et al. 2011).

Note that the mean activity level reported in Johnson et al. (2011) using the HIRES spectrograph is S_{MW} = 0.128 $\pm$ 0.014 The uncertainty is taken to be 11 %, as reported for the HIRES calibration to the Mount Wilson system (Isaacson & Fischer 2010). The difference between this S_{MW} value and our measurement (Table 3) is at the 1.5 σ level, i.e. not significant.

4.4.3 WASP-103

WASP-103b is an extreme HJ, close to tidal disruption (Gillon et al. 2014; Southworth et al. 2014). The S_{RSS} RMS

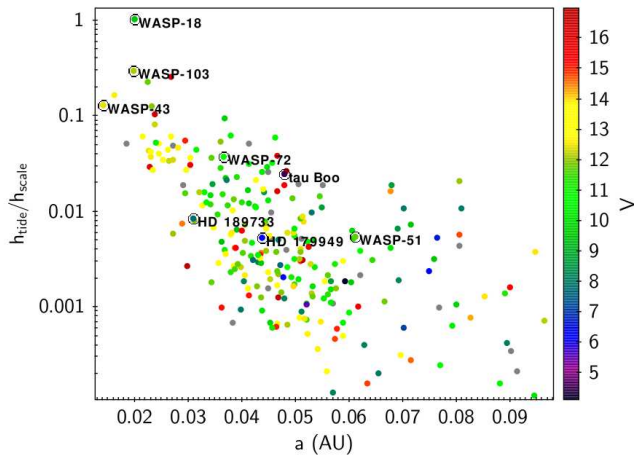

Figure 8. SPI interaction strength proxies for planets with $M_{\rm p}\sin i$ = 0.1-13 $M_{\rm J}$ and a < 0.1 AU. The visual magnitude is shown as a guide to the observability of the systems. Planets observed in this study and key systems from the literature are labelled. A null-result for SPI in the particularly extreme WASP-18 system was found by Miller et al. (2012), and attributed to the very low intrinsic activity level of this F6V star; see X-ray nondetection in Pillitteri et al. (2014). Evidence for weak SPI effects have been reported for HD 179949 (Shkolnik et al. 2003), HD 189733 (Poppenhaeger & Wolk 2014) and tau Boo (Walker et al. 2008).

variability over our 16 observations of WASP-103 is at the 2 % level, comparable to the photon noise uncertainties. We saw no significant changes in the Ca II H & K line core profiles, though the data sample a narrow phase range away from transit, so we are unable to address the issue of phase-dependent absorption. The dispersion in $\log(R'_{\rm HK})$ is 0.02. This is lower than the uncertainties quoted for individual values, since those include additional systematic calibration and B-V uncertainties.

Our mean $\log(R'_{\rm HK})$ value of -4.57 corresponds to a low activity-age compared with alternative estimates (Table 3), but the significance of the age difference is only high with respect to the Gillon et al. (2014) age estimate (3 σ). Improved stellar parameters are needed for a better constrained independent age assessment (c.f. Table 6 in Southworth et al. 2014). By analogy with WASP-12 (Fossati et al. 2010; Haswell et al. 2012) we expected depressed activity due to absorption by circumstellar gas from the extreme HJ planet. Either this is masked by SPI or the planetary mass loss rate may be unexpectedly low. Modelling of atmospheric escape, as for WASP-43, would be useful to investigate this possibility. Figure 8 suggests SPI enhancements are plausible. WASP-103 has the second-highest tidal interaction proxy value h_{tide}/h_{scale} of all known exoplanets. The value is a third of the extreme WASP-18 system, for which the possibility of tidal activity suppression rather than enhancement has been invoked (Pillitteri et al. 2014).

4.4.4 *WASP-72*

WASP-72 is among the most highly irradiated hot Jupiters known (Gillon et al. 2013). Our measured activity value falls below the basal level, see Figure 5 and 6. While the uncertainty on $\log(R'_{\rm HK})$ is relatively large, WASP-72 certainly falls amongst the lowest activity outliers for both main sequence and evolved stars of its spectral type. In Figure 6 we show the substantial uncertainty contribution from the calibration to the Mount Wilson system. Note that intercomparing activity values measured with the same instrument setup does not suffer this systematic uncertainty. $\log(R'_{\rm HK})$ implies WASP-72 is far older than stellar evolution models suggest (Table 3, MH08), strengthening the case for a depressed activity value. We conclude WASP-72 is a system where relatively weak Ca II H & K emission from an inactive, ∼3 Gyr old star (Gillon et al. 2013) is absorbed sufficiently to appear below the basal limit, analogously to other close-in planet systems (Lanza 2014; Fossati et al. 2015a). With currently available data for the WASP-72 system, we cannot disentangle circumstellar absorption from planetary mass loss and absorption in the ISM. However, our estimates in Section 4.3 indicate the known ISM clouds along the line of sight (Table 4) cannot entirely explain the anomalously low value even if the intrinsic stellar emission is exactly at the basal level.

5 CONCLUSIONS

We calibrated the RSS at SALT to measure chromospheric activity on the Mount Wilson system. We used this to measure the activity of four HJ host stars. Fossati et al. (2013) highlighted the anomalously low $\log(R'_{\rm HK})$ values for WASP-12 and five other planet hosts included in Knutson et al. (2010). We revisit this with the significantly extended dataset of Figueira et al. (2014), finding that 24 % of the sample (22 hosts) show these anomalies including two low mass, multi-planet systems and WASP-72 (Figs. 5 and 6).

WASP-43 is an outlier in the opposite corner of Fig. 5, while WASP-51/HAT-P-30 has an anomalously low $\log(R'_{\rm HK})$ for its age. There may be (at least) two processes operating in close-in HJ systems which affect the observed $\log(R'_{\rm HK})$ values. Anomalously high $\log(R'_{\rm HK})$ values may be attributed to SPI (Cuntz et al. 2000). The outliers in the bottom left of Fig. 5 can be attributed to diffuse circumstellar gas lost from the planets which absorbs the stellar chromospheric emission in strong resonance lines (Haswell et al. 2012; Fossati et al. 2013). Absorption by the ISM may also play a role for some of these systems. Our estimates suggest the latter cannot explain the anomalous values of WASP-51 and WASP-72. Further investigations are needed to examine any interstellar and circumstellar absorption contributions, and to test whether the intrinsic activity levels of WASP-72 and WASP-51 are indeed normal.

Further measurements are needed to investigate whether WASP-43's anomalously high $\log(R'_{\rm HK})$ is time-dependent. The extreme HJ WASP-103 b also displays higher activity than expected from the system age; improved stellar parameters are needed to test this conclusion. WASP-43 and WASP-103 have exceptionally high predicted SPI levels from the simple scaling laws illustrated in Fig. 8.

A quarter of the host stars of short period exoplanets exhibit anomalously low values of $\log(R'_{\rm HK})$. Activity can appear depressed by circumstellar absorption of the stellar Ca II H & K flux. SPI can potentially enhance the normal Ca II H & K emission. In some systems, including WASP-

103, both mechanisms may operate simultaneously. Such systems would not necessarily have obviously anomalous $\log(R'_{\rm HK})$ activity ages. We recommend that the $\log(R'_{\rm HK})$ index is never used as an age indicator for stars which host close-in planets: it is unreliable for this purpose. Disentangling the mechanisms to the extent of being able to predict which one dominates will require extensive uniform observational work, covering a range of stellar spectral types, ages, planet masses, planet radii, Roche lobe radii, orbital separations, and measurements of the stellar magnetic field configurations.

ACKNOWLEDGMENTS

All of the observations reported in this paper were obtained with the Southern African Large Telescope (SALT), in which the Open University is a shareholder, as part of the UK SALT Consortium. We thank the SALT astronomers for making our observations, Geoff Bradshaw for IT support, in particular for OU undergraduate GS, and CH thanks M. Williams and R. Gandhi-Patel for logistical support. DS is supported by an STFC studentship, CAH and JRB are supported by STFC under grant ST/L000776/1. This research has made use of the SIMBAD database, operated at CDS, Strasbourg, France.

REFERENCES

Anderson E., Francis C., 2012, Astron. Lett., 38, 331
Arriagada P., 2011, ApJ, 734, 70
Baliunas S. L., et al., 1995, ApJ, 438, 269
Balona L. A., 2015, MNRAS, 447, 2714
Ben-Jaffel L., Ballester G. E., 2013, A&A, 553, A52
Bisikalo D., Kaygorodov P., Ionov D., Shematovich V., Lammer H., Fossati L., 2013, ApJ, 764, 19
Bonfanti A., Ortolani S., Piotto G., Nascimbeni V., 2015, A&A, 575, A18
Bourrier V., et al., 2013, A&A, 551, A63
Buckley D. A. H., Swart G. P., Meiring J. G., 2006, in Stepp L. M., ed., Vol. 6267, Ground-based a. Airborne Telesc.. pp 62670Z–62670Z–15, doi:10.1117/12.673750, http://adsabs.harvard.edu/abs/2006SPIE.6267E..32B
Canto Martins B. L., das Chagas M. L., Alves S., Leão I. C., de Souza Neto L. P., de Medeiros J. R., 2011, A&A, 530, A73
Carilli C., Rawlings S., 2004, New Astronomy Reviews, 48, 979
Chadney J., Galand M., Unruh Y., Koskinen T., Sanz-Forcada J., 2015, Icarus, 250, 357
Cohen O., Kashyap V. L., Drake J. J., Sokolov I. V., Garraffo C., Gombosi T. I., 2011, ApJ, 733, 67
Crawford S. M., et al., 2010, in Silva D. R., Peck A. B., Soifer B. T., eds, Vol. 7737, Proc. SPIE. pp 773725–773725–12, doi:10.1117/12.857000, http://adsabs.harvard.edu/abs/2010SPIE.7737E..54C
Cuntz M., Saar S. H., Musielak Z. E., 2000, ApJ, 533, L151
Czesla S., Salz M., Schneider P. C., Schmitt J. H. M. M., 2013, A&A, 560, A17
Duncan D. K., et al., 1991, ApJS, 76, 383
Ehrenreich D., et al., 2015, Nature, 522, 459
Enoch B., et al., 2011, AJ, 142, 86
Erkaev N. V., Kulikov Y. N., Lammer H., Selsis F., Langmayr D., Jaritz G. F., Biernat H. K., 2007, A&A, 472, 329
Figueira P., Oshagh M., Adibekyan V. Z., Santos N. C., 2014, A&A, 572, A51
Figueira P., et al., 2016, A&A, 592, A143
Fossati L., et al., 2010, ApJ, 714, L222
Fossati L., Ayres T. R., Haswell C. A., Bohlender D., Kochukhov O., Flöer L., 2013, ApJ, 766, L20
Fossati L., Ingrassia S., Lanza A. F., 2015a, ApJ, 812, L35
Fossati L., France K., Koskinen T., Juvan I. G., Haswell C. A., Lendl M., 2015b, ApJ, 815, 118
Gillon M., et al., 2013, A&A, 552, A82
Gillon M., et al., 2014, A&A, 562, L3
Gomes da Silva J., Santos N. C., Boisse I., Dumusque X., Lovis C., 2014, A&A, 566, A66
Gray R. O., Corbally C. J., Garrison R. F., McFadden M. T., Robinson P. E., 2003, AJ, 126, 2048
Gray R. O., Corbally C. J., Garrison R. F., McFadden M. T., Bubar E. J., McGahee C. E., O'Donoghue a. a., Knox E. R., 2006, AJ, 132, 161
Hall J. C., Lockwood G. W., Skiff B. a., 2007, AJ, 133, 862
Han E., Wang S. X., Wright J. T., Feng Y. K., Zhao M., Fakhouri O., Brown J. I., Hancock C., 2014, PASP, 126, 827
Hartman J. D., 2010, ApJ, 717, L138
Haswell C. A., et al., 2012, ApJ, 760, 79
Hellier C., et al., 2011, A&A, 535, L7
Hernán-Obispo M., Gálvez-Ortiz M. C., Anglada-Escudé G., Kane S. R., Barnes J. R., de Castro E., Cornide M., 2010, A&A, 512, A45
Hernán-Obispo M., et al., 2015, A&A, 576, A66
Hewitt Â., 2011, American Astronomical Society, 43
Isaacson H., Fischer D., 2010, ApJ, 725, 875
Jenkins J. S., et al., 2006, MNRAS, 372, 163
Jenkins J. S., Jones H. R. a., Pavlenko Y., Pinfield D. J., Barnes J. R., Lyubchik Y., 2008, A&A, 485, 571
Jenkins J. S., et al., 2011, A&A, 531, A8
Jin S., Mordasini C., Parmentier V., van Boekel R., Henning T., Ji J., 2014, ApJ, 795, 65
Johnson J. A., et al., 2011, ApJ, 735, 24
Knutson H. A., Howard A. W., Isaacson H., 2010, ApJ, 720, 1569
Kobulnicky H. A., Nordsieck K. H., Burgh E. B., Smith M. P., Percival J. W., Williams T. B., O'Donoghue D., 2003, in Iye M., Moorwood A. F. M., eds, Vol. 4841, Instrument Design and Performance for Optical/Infrared Ground-based Telescopes. Edited by Iye. pp 1634–1644, doi:10.1117/12.460315, http://adsabs.harvard.edu/abs/2003SPIE.4841.1634K
Koskinen T., Harris M., Yelle R., Lavvas P., 2013, Icarus, 226, 1678
Krejčová T., Budaj J., 2012, A&A, 540, A82
Kulow J. R., France K., Linsky J., Parke Loyd R. O., 2014, ApJ, 786, 132
Kurokawa H., Nakamoto T., 2014, ApJ, 783, 54
Kurucz R. L., Furenlid I., Brault J., Testerman L., 1984, National Solar Observatory Atlas
Lammer H., Selsis F., Ribas I., Guinan E. F., Bauer S. J., Weiss W. W., 2003, ApJ, 598, L121
Lanza A. F., 2008, A&A, 487, 1163
Lanza A. F., 2012, A&A, 544, A23
Lanza A. F., 2013, A&A, 557, A31
Lanza A. F., 2014, A&A, 572, L6
Lecavelier des Etangs A., et al., 2010, A&A, 514, A72
Lenz L. F., Reiners A., Kürster M., 2011, in 16th Cambridge Work. on Cool Stars. http://adsabs.harvard.edu/abs/2011ASPC..448.1173L
Linsky J. L., Yang H., France K., Froning C. S., Green J. C., Stocke J. T., Osterman S. N., 2010, ApJ, 717, 1291
Lopez E. D., Fortney J. J., Miller N., 2012, ApJ, 761, 59
Lovis C., et al., 2011, preprint (arXiv:1107.5325)
Lundkvist M. S., et al., 2016, Nature Communications, 7, 11201
Maggio A., et al., 2015, ApJ, 811, L2
Mamajek E. E., Hillenbrand L. a., 2008, ApJ, 687, 1264
Matsakos T., Königl A., 2016, ApJ, 820, L8
Matsakos T., Uribe A., Königl A., 2015, A&A, 578, A6

Miller B. P., Gallo E., Wright J. T., Dupree A. K., 2012, ApJ, 754, 137
Miller B. P., Gallo E., Wright J. T., Pearson E. G., 2015, ApJ, 799, 163
Mittag M., Schmitt J. H. M. M., Schröder K.-P., 2013, A&A, 549, A117
Noyes R. W., Hartmann L. W., Baliunas S. L., Duncan D. K., Vaughan A. H., 1984, ApJ, 279, 763
Pace G., 2013, A&A, 551, L8
Partnership A., et al., 2015, ApJ, 808, L1
Paulson D. B., Saar S. H., Cochran W. D., Hatzes A. P., 2002, AJ, 124, 572
Pillitteri I., Günther H. M., Wolk S. J., Kashyap V. L., Cohen O., 2011, ApJ, 741, L18
Pillitteri I., Wolk S. J., Sciortino S., Antoci V., 2014, A&A, 567, A128
Poppenhaeger K., Schmitt J. H. M. M., 2011, ApJ, 735, 59
Poppenhaeger K., Wolk S. J., 2014, A&A, 565, L1
Poppenhaeger K., Robrade J., Schmitt J. H. M. M., 2010, A&A, 515, A98
Redfield S., Linsky J. L., 2008, ApJ, 673, 283
Salz M., Czesla S., Schneider P. C., Schmitt J. H. M. M., 2016, A&A, 586, A75
Saur J., Grambusch T., Duling S., Neubauer F. M., Simon S., 2013, A&A, 552, A119
Scharf C. A., 2010, ApJ, 722, 1547
Schröder K.-P., Mittag M., Pérez Martínez M. I., Cuntz M., Schmitt J. H. M. M., 2012, A&A, 540, A130
See V., Jardine M., Fares R., Donati J.-F., Moutou C., 2015, MNRAS, 450, 4323
Sekiguchi M., Fukugita M., 2000, AJ, 120, 1072
Shkolnik E., Walker G. A. H., Bohlender D. A., 2003, ApJ, 597, 1092
Shkolnik E., Bohlender D. A., Walker G. A. H., Collier Cameron A., 2008, ApJ, 676, 628
Southworth J., 2011, MNRAS, 417, 2166
Southworth J., et al., 2014, MNRAS, 447, 711
Strugarek A., Brun A. S., Matt S. P., Réville V., 2015, ApJ, 815, 111
Vidal-Madjar A., Des Etangs A. L., Désert J.-M., Ballester G. E., Ferlet R., Hébrard G., Mayor M., 2003, Nature, 422, 143
Vidotto A. A., Fares R., Jardine M., Moutou C., Donati J.-F., 2015, MNRAS, 449, 4117
Walker G. A. H., et al., 2008, A&A, 482, 691
Welsh B. Y., Lallement R., Vergely J.-L., Raimond S., 2010, A&A, 510, A54
Wilson O. C., 1968, ApJ, 153, 221
Wright J. T., 2004, AJ, 128, 1273
van Haarlem M. P., et al., 2013, A&A, 556, A2

This paper has been typeset from a TEX/LATEX file prepared by the author.